Supplementary Material
to
"Native-oxide limited cross-plane thermal transport in suspended silicon membranes revealed by scanning thermal microscopy"

A.M. Massoud[a,b †], J.-M. Bluet[a], V. Lacatena[c,d], M. Haras[c], J.-F. Robillard[c], P-O. Chapuis[b]

[a] Univ Lyon, Institut des Nanotechnologies de Lyon (INL), CNRS, INSA de Lyon, F-69621 Villeurbanne, France.
[b] Univ Lyon, CNRS, INSA-Lyon, Université Claude Bernard Lyon 1, CETHIL UMR5008, F-69621, Villeurbanne, France.
[c] Univ. Lille, CNRS, Centrale Lille, ISEN, Univ. Valenciennes, UMR 8520 - IEMN, F-59000 Lille, France.
[d] STMicroelectronics, 850, rue Jean Monnet, F-38926 Crolles, France.

1. Heat conduction at the contact and below

The thermal conductance from a circular surface of radius b to a bulk semi-infinite material of thermal conductivity λ can be written as[1]

$$G_{bulk} = 4b\lambda. \quad \text{(S1)}$$

The thermal conductance in the effective medium of conductivity λ_{eff} representing the multilayer (see inset of Fig. 4) can therefore be determined if the thermal contact radius b is known. This quantity is key to the interpretation of SThM experiments and has been evaluated from theoretical considerations in many papers[2-5]. By varying both this contact radius b_{test} and the membrane thermal conductivity $\lambda_{m,test}$, we are able to obtain the thermal conductance associated to the dissipation from the contact in the sample $G_{multilayer}(\lambda_{m,test}, b_{test})$. This can be performed analytically or, in our case, numerically with FEM. Eq. (S1) allows to obtain $\lambda_{eff}(\lambda_{m,test}, b_{test})$ from G. We apply then the calibration curve of Fig. 2, but where the air contribution simulated with FEM has been subtracted ($\Delta\theta_{contact} = \Delta\theta - \Delta\theta_{air,FEM}$)[6]. As a result, we compute

$$\begin{aligned}&\Delta\theta(\lambda_{m,test}, b_{test})\\ &= \Delta\theta_{air}(\lambda_{m,test}) + \Delta\theta_{contact}(\lambda_{m,test}, b_{test})\end{aligned} \quad \text{(S2)}$$

in Fig. 4 of the main part of the paper.

2. Effect of the tip-sample minimal distance considered in FEM

Using FEM simulations we can only solve the heat diffusion equation. It is known that less heat transfer takes place in the ballistic regime, so the tip should not be located too close to the sample in the FEM simulations in order to avoid an overestimation of the probe-sample thermal

exchange through air. In order to account for the ballistic limit to the transfer, we calculated the minimal distance at which the tip should be set in the FEM simulations and found it to be equal to 4 Λ_a[6]. As a consequence, the tip is placed at d_0 = 240 nm above the sample, because this is the limit between the diffusive and the ballistic regimes[7]. As the actual value may depart slightly from this value, we test the dependence to the distance by performing simulations with the tip closer to the sample surface, at 210 nm (see Suppl. Fig. S1). We compute $\Delta\theta_{air}$ from a 3D FEM simulation at the new tip-sample minimal height 210 nm (note $\Delta\theta_{contact}$ is not affected by the variation of d). A similar curve as that of Fig. 4 leads to a contact radius b=287 nm, very close to the value 285 nm found for d=240 nm, which induces an uncertainty of 0.3 W.m^{-1}.K^{-1} on λ_m. The sensitivity to d_0 stays therefore limited.

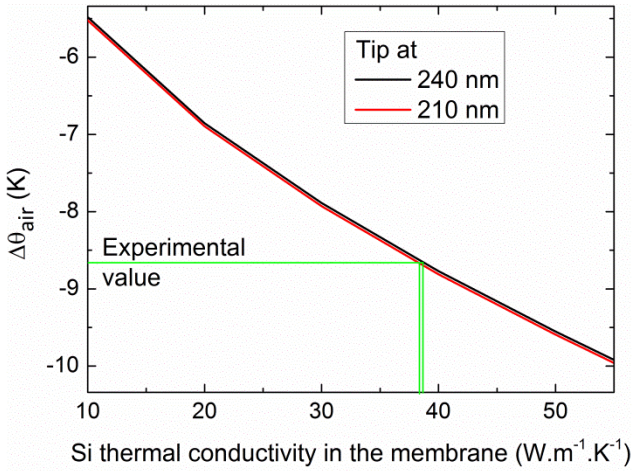

Suppl. Fig. S1. Simulated tip temperature decrease as a function of silicon thermal conductivity in the membrane. The tip-sample minimal distances are respectively 210 nm and 240 nm above the sample.

3. Effect of the air cavity depth

In order to probe the depth of the air cavity between the membrane and the substrate, we performed profilometry measurements. The uncertainty on these measurements is $\pm$ 1 µm. Suppl. Fig. S2(a) depicts the simulated tip temperature decrease through air as a function of the silicon thermal conductivity in the membrane. It shows that accounting for such uncertainty has a weak effect on the tip temperature decrease, lower than 50 mK. Suppl. Fig. S2(b) depicts the simulated thermal conductance G in the 2D axisymmetric model modeling heat conduction at the contact. It shows that the relative variations in G are smaller than 1% which induce an uncertainty smaller than 0.1 W.m^{-1}.K^{-1} on λ_m. All these results confirm the obtaining of plateaus, while probing the membrane, in the experimental profiles.

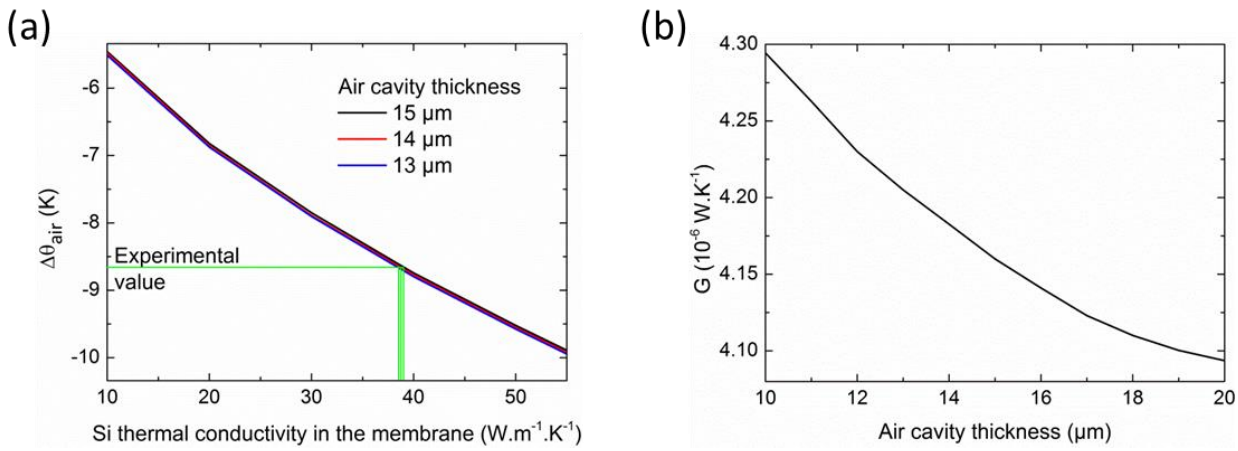

Suppl. Fig. S2. Air cavity effect. (a) Simulated tip temperature decrease as a function of the silicon thermal conductivity in the membrane. (b) Simulated thermal conductance as a function of the air cavity thickness for silicon membrane thermal conductivity λ_m= 60 W.m^{-1}.K^{-1} and thermal radius b = 285 nm.

4. Temperature profiles simulated with Finite Element Modeling

Suppl. Fig. S3 shows the effect of the 1.5 nm thick native oxide layers on the simulated temperature profiles within the membrane, as a result of the heat exchanged between the tip and the sample. We consider also the case where the native oxide layers are replaced with thermal boundary resistances ρ_{CP} = (1.5×10^{-9} m)/(1.5 W.m^{-1}.K^{-1}) = 1×10^{-9} m^2.K.W^{-1}, accounting only for the cross-plane heat transfer. The results in Suppl. Fig. S3 show the strong difference in temperature profiles in the three cases (membrane, membrane with layer, membrane with boundary resistance). Note that here the temperature fields are analyzed, and not anymore the tip average temperature decrease. The heat transfer though the air and at the contact are successively addressed.

The probe temperature rise is set 100 K above ambient in the 3D simulation of Suppl. Fig. S3(a), which describes the heat transfer due to the air and where the sample temperature is found to be lower. Most importantly, it can be seen that considering oxide layers leads to a lower temperature in the membrane in comparison to the case of boundary resistances. This is due to the fact that both in-plane and cross-plane heat conduction should be considered (see also Suppl. Fig. S4(a)).

In the case of the contact heat transfer (Suppl. Fig. S3(b)), the membrane surface is set (arbitrarily) at 100 K above ambient. Analyzing the case where the surface effects are accounted for through boundary resistances (blue curve), it can be observed that the drop in temperature is larger at the top surface than at the bottom surface. The temperature drop in the oxide film of the top surface seems also to be larger than that of the bottom surface. In both cases the drop is limited at the bottom surface of the membrane, due to the strong in-plane nature of the transport taking place close to the insulating air layer: heat flux lines are not perpendicular to the

membrane in the second native oxide layer (see Suppl. Fig. S4(b)) and the jump in the temperature profile cannot be seen easily. In order to observe this temperature jump ρ_{CP} needs to be replaced by $100\rho_{CP}$ as shown in Suppl. Fig. S5, where the temperature discontinuity is still modest despite the huge resistance considered.

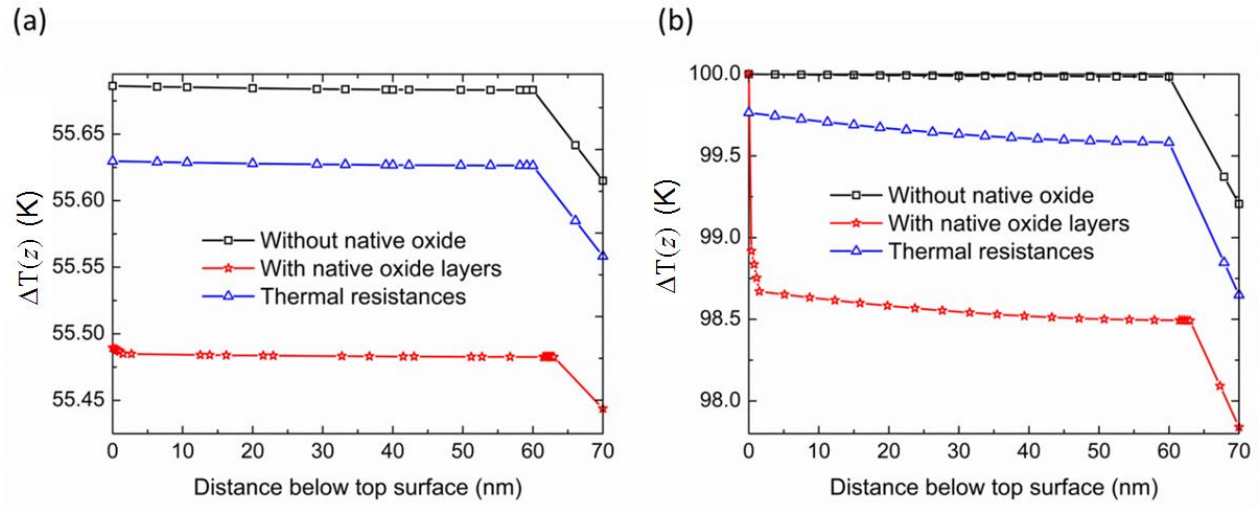

Suppl. Fig. S3. Temperature profile within the sample. (a) Temperature within the membrane due to heating through the air heat transfer, simulated with FEM in a 3D configuration as in Fig. 3. (b) Temperature within the membrane due to heating at the contact, simulated with FEM in a 2D axisymmetric configuration. The contact temperature rise is set to 100 K (along the radius b) above ambient.

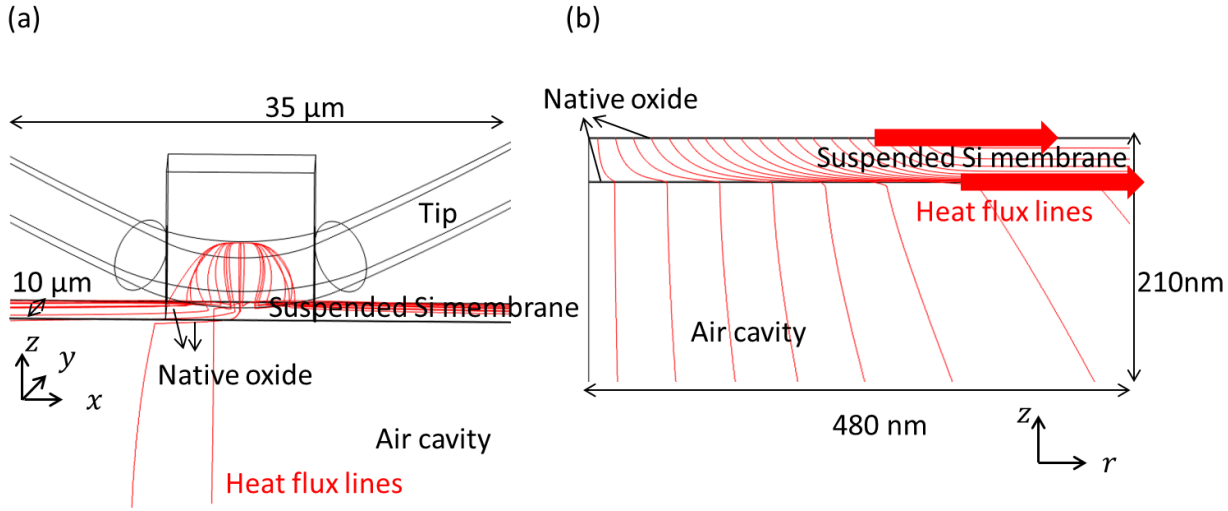

Suppl. Fig. S4. Heat flux lines. (a) Heat transfer through air modeled with FEM in a 3D configuration. Note that this is a 3D representation and not a cross-section, therefore the width of the membrane is observed (and not its thickness). (b) Heat conduction below the contact modeled with FEM in 2D axisymmetric configuration. Note that the scale is different on the vertical and horizontal axes.

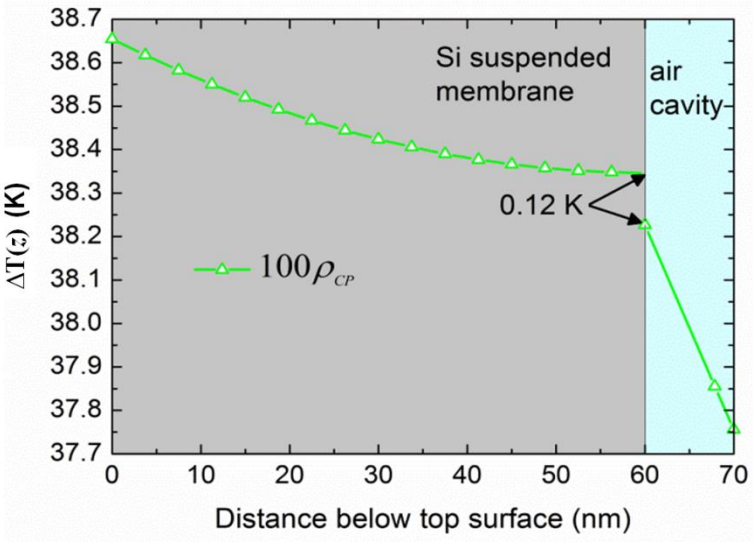

Suppl. Fig. S5. Temperature within the membrane due to heating at the contact, simulated with FEM in a 2D axisymmetric configuration using a boundary resistance of $100\rho_{CP}$. The contact temperature rise is set to 100 K (along the radius b) above ambient.

5. Thermal boundary resistance

In order to determine the thermal boundary resistance ρ allowing to reproduce the experimental data, we simulate the heat transfer through the air with FEM in the 3D configuration (see Suppl. Fig. S6(a)) and at the contact with FEM in a 2D axisymmetric configuration (see Suppl. Fig. S6(b)) by replacing the native oxide layers with ρ_{TBR}. We find ρ_{TBR} ~ 30×10^{-9} $m^2.K.W^{-1}$, which is 30 times larger than the cross-plane thermal boundary resistance ρ_{CP}.

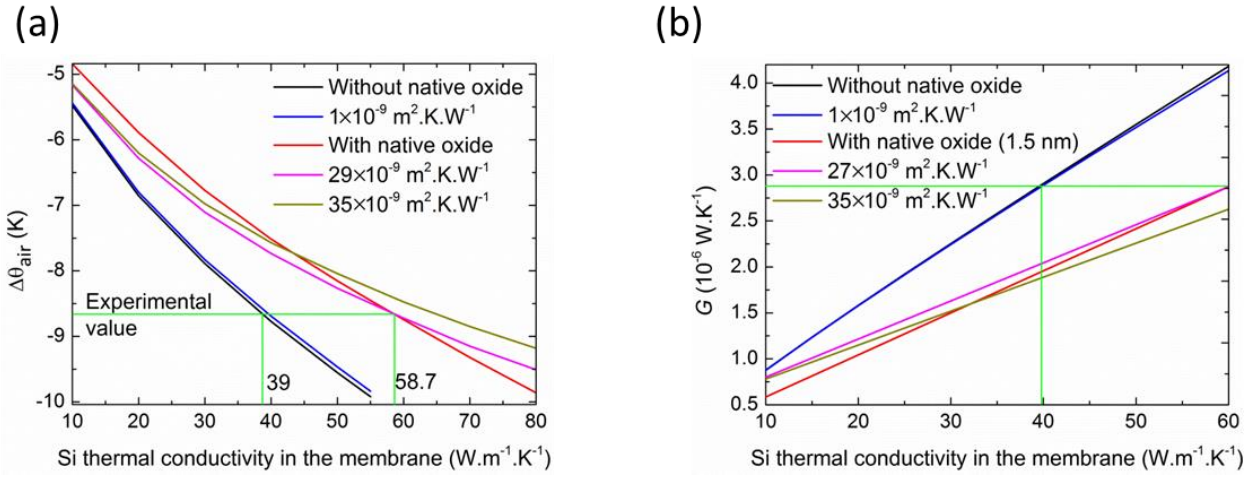

Suppl. Fig. S6. Tip temperature decrease as a function of the silicon thermal conductivity in the

membrane for various thermal boundary resistances. (a) Simulated tip temperature decrease as a function of silicon thermal conductivity in the membrane. (b) Simulated thermal conductance as a function of silicon thermal conductivity in the membrane. λ_m= 60 W.m^{-1}.K^{-1}, b = 285 nm.

6. Limitations of the FEM models

All the simulations presented in this work consider heat diffusion with reduced thermal conductivity in the silicon membrane. An improved step, beyond the scope of this paper, would be to include fully the ballistic transport within the membrane.

References

[S1] S. Lefèvre and S. Volz, *Rev. Sci. Instrum*, 76, 3 (2005).

[S2] J. Bodzenta, J. Juszczyk, A. Kaźmierczak-Bałata, P. Firek, A. Fleming and M. Chirtoc, *Int. J. Thermophys.*, 37, 10 (2016).

[S3] S. Lefèvre, S. Volz, J.-B. Saulnier, C. Fuentes and N. Trannoy, *Rev. Sci. Instrum.*, 74, 4 (2003).

[S4] K. Kim, W. Jeong, W. Lee, S. Sadat, D. Thompson, E. Meyhofer and P. Reddy, *Appl. Phys. Lett.*, 105, 20 (2014).

[S5] Y. Zhang, E. E. Castillo, R. J. Mehta, G. Ramanath and T. Borca-Tasciuc, *Rev. Sci. Instrum.*, 82, 2 (2011).

[S6] A.M. Massoud, J.-M. Bluet, P-O. Chapuis, Air contribution in calibrated microprobe based scanning thermal microscopy, submitted (2017).

[S7] L. Shi and A. Majumdar, *J. Heat Transf.*, 124, 329–337 (2002).